Growth and Structural Characterization of $Rb_3Yb_2(PO_4)_3$: A New Material for Laser and Nonlinear Optical Applications

J. J. Carvajal,† I. Parreu,† R. Solé,† X. Solans,‡ F. Díaz,† and M. Aguiló*,†

Física i Cristal·lografia de Materials (FiCMA), Universitat Rovira i Virgili, Campus Sescelades, 43007 Tarragona, Spain, and Departament de Cristal·lografia i Mineralogía, Universitat de Barcelona, 08028 Barcelona, Spain

Received June 15, 2005. Revised Manuscript Received October 13, 2005

We report the synthesis of a new stoichiometric Yb compound, $Rb_3Yb_2(PO_4)_3$, by high-temperature solution methods. This is the first material of the $A_3^IB_2^{III}(X^VO_4)_3$ family containing a lanthanide element and the only one that shows optical activity. We resolved the structure of $Rb_3Yb_2(PO_4)_3$, which crystallize in the cubic system, space group of symmetry $I2_13$ ($a = 16.8700(10)$ Å, $Z = 16$), and studied its evolution with the temperature. The thermal expansion coefficient of $Rb_3Yb_2(PO_4)_3$ is $\alpha = 8.94 \times 10^{-6}$ K^{-1}. This compound melts incongruently at 1450 K. The second-harmonic generation efficiency of the $Rb_3Yb_2(PO_4)_3$, although limited as a result of the crystal not presenting birefringence, was at least similar to that of potassium dihydrogen phosphate.

Introduction

When we studied how changing the concentration of Nb_2O_5 and Yb_2O_3 affects the crystallization region of $RbTiOPO_4$, we identified different neighboring phases to $RbTiOPO_4$ with a high content of ytterbium.[1] In solutions containing 43.1% of Rb_2O, 31.9% of P_2O_5, and 25.0% of TiO_2 (with the partial substitution of this component by Nb_2O_5 and Yb_2O_3), we identified the $Rb_2Ti_{2-x-y}Yb_xNb_y(PO_4)_3$ phase ($x = 1.02-1.43$; $y = 0.00-0.29$),[2] which has a langbeinite-type structure. But, when the solution contained 40.8% of Rb_2O, 27.2% of P_2O_5, and 32.0% of TiO_2 (again, with the partial substitution of this component by Nb_2O_5 and Yb_2O_3), a new phase was identified as $Rb_3Yb_2(PO_4)_3$ in addition to the langbeinite-type structure mentioned above.

New Yb-stoichiometric materials are interesting because of their wide range of applications, which include magnetic, superconductor, and solid-state laser materials.[3] Interest in them increases when their structure is non-centrosymmetric because of the possibility of generating self-frequency doubling output of the Yb^{3+} emission at around 1 μm, obtaining laser emission in the green.

The structures of $A_3^IB_2^{III}(X^VO_4)_3$ oxides belong to different spatial groups of symmetry. The phosphates (X = P) with B = Al have been widely studied because of their adsorption and catalytic properties.[4] Most aluminum phosphates, those containing Na (A = Na), have been widely studied since the discovery by Hong et al.[5,6] of fast Na^+-ion transport properties in the nasicon system. Numerous phosphates of similar composition have since been synthesized to study the correlation between the structure and the cations occupying A, B, and X positions.[4,7,8] We should also mention the number of compounds containing Li (A = Li), which seem to be promising materials for use as solid electrolytes in a solid lithium battery.[8] However, none of these compounds exhibit the non-centrosymmetric structure of the $Rb_3Yb_2(PO_4)_3$.

In this paper we report the obtaining, crystal growth, and X-ray single-crystal structure of $Rb_3Yb_2(PO_4)_3$, which crystallizes in a new cubic structure type for $A_3B_2(XO_4)_3$ oxides, and describe how this structure evolves with temperature. We also analyze the nonlinear optical properties of these crystals.

Experimental Procedures

Synthesis and Identification of Crystalline Phases. Crystals of $Rb_3Yb_2(PO_4)_3$ were synthesized from high-temperature solutions. The crystalline phases were obtained by growth experiments carried out in a single-zone vertical tubular furnace equipped with a Kanthal AF heater. The temperature of the furnace, measured near the heater with an S-type Pt−Pt 10% Rh thermocouple, was controlled with a Eurotherm 818P controller/programmer connected to a thyristor.

The synthesis was carried out in solutions prepared in conical Pt crucibles of 25 cm^3 of volume. These solutions, weighing 15−20 g, were prepared by mixing the desired amounts of Rb_2CO_3, $NH_4H_2PO_4$, TiO_2, Yb_2O_3, and Nb_2O_5 (p.a.) in agreement with Table 1. The Nb_2O_5 was introduced because it was demonstrated to increase the content of rare earths in $RbTiOPO_4$ crystals doped with rare earths.[1] $Rb_3Yb_2(PO_4)_3$ crystals were obtained as a boundary

* Corresponding author. E-mail: magdalena.aguilo@urv.net.
† Universitat Rovira i Virgili.
‡ Universitat de Barcelona.

(1) Carvajal, J. J.; Nikolov, V.; Solé, R.; Gavaldà, Jna. Massons, J.; Aguiló, M.; Díaz, F. *Chem. Mater.* **2002**, *14*, 3136.
(2) Carvajal, J. J.; Aznar, A.; Solé, R.; Gavaldà, Jna.; Massons, J.; Solans, X.; Aguiló, M.; Díaz, F. *Chem. Mater.* **2003**, *15*, 204.
(3) Pujol, M. C.; Bursukova, M. A.; Güell, F.; Mateos, X.; Solé, R.; Gavaldà, Jna.; Aguiló, M.; Massons, J.; Díaz, F.; Klopp, P.; Griebner, U.; Petrov, V. *Phys. Rev. B* **2002**, *65*, 165121.
(4) Lii, K. H.; Ye, J. *J. Solid State Chem.* **1997**, *131*, 131.
(5) Hong, H. Y.-P. *Mater. Res. Bull.* **1976**, *11*, 173.
(6) Goodenough, J. B.; Hong, H. Y.-P.; Kafalas, J. A. *Mater. Res. Bull.* **1976**, *11*, 203.
(7) Masquelier, C.; d'Yvoire, F.; Collin, G. *J. Solid State Chem.* **1995**, *118*, 33.
(8) d'Yvoire, F.; Pintard-Scrépel, M.; Bretey, E.; de la Rochère, M. *Solid State Ionics* **1983**, *9−10*, 851.

10.1021/cm0512934 CCC: $30.25
Published on Web 11/19/2005

Table 1. Solution Compositions Studied and Chemical Compositions of the Crystals Obtained

	solution composition (mol %)					
expt no.	Rb_2O	P_2O_5	TiO_2	Yb_2O_3	Nb_2O_5	crystal composition
1	40.8	27.2	29.44	2.24	0.32	$RbTiOPO_4$
2	40.8	27.2	29.12	2.56	0.32	$Rb_3Yb_2(PO_4)_3$
3	40.8	27.2	29.12	1.92	0.96	$RbTiOPO_4$
4	40.8	27.2	28.8	2.24	0.96	$Rb_3Yb_2(PO_4)_3$
5	40.8	27.2	28.48	2.56	0.96	$Rb_3Yb_2(PO_4)_3$
6	40.8	27.2	29.44	1.28	1.28	$RbTiOPO_4$
7	40.8	27.2	29.12	1.60	1.28	$RbTiOPO_4$ + $Rb_{1.97}Ti_{0.48}Yb_{1.38}Nb_{0.14}(PO_4)_3$
8	40.8	27.2	28.8	1.92	1.28	$Rb_{1.97}Ti_{0.45}Yb_{1.43}Nb_{0.12}(PO_4)_3$

phase of the crystallization region of $RbTiOPO_4$ in the $Rb_2O-P_2O_5-TiO_2$ system, with a partial substitution of TiO_2 by Yb_2O_3 or combinations of Nb_2O_5 and Yb_2O_3. The solution compositions used to synthesize this new compound and its neighboring phases $Rb_2Ti_{2-x-y}Yb_xNb_y(PO_4)_3$ and $RbTiOPO_4$:(Nb,Yb) are shown in Table 1. The solutions were heated at 1273 K to homogenize them and maintained at a temperature of about 50−100 K above the expected saturation temperature for 3−5 h. When the solution was homogeneous, we decreased the temperature at a rate of 10 K every 30 min until spontaneous crystallization appeared on a platinum wire immersed in the solution. We then decreased the temperature between 10 and 50 K at a rate of 1−5 K/h to obtain a higher amount of macroscopic crystals. Transparent, faceted $Rb_3Yb_2(PO_4)_3$ crystals of a maximum linear dimension of 2 mm were then obtained.

The crystallized phase was preliminary identified by direct observation in an optical microscope. We then identified it by X-ray powder diffraction analyses using a Siemens D-5000 X-ray powder diffractometer. The stoichiometry of the obtained crystals was analyzed by electron probe microanalysis (EPMA). The morphology of the crystals was observed and photographed by scanning electron microscopy (SEM) in a JEOL JSM 6400 scanning electron microscope.

EPMA Measurements. We analyzed the chemical composition of the crystals obtained by EPMA, operating in wavelength-dispersion spectroscopy, in a CAMECA SX-50. The analyses were carried out at 25 kV accelerating voltage and 30 nA electron current for Rb, Ti, P, and O and 100 nA for Yb and Nb. As standards we used a $RbTiOPO_4$ crystal, grown by us, for measuring Rb, Ti, P, and O, YbF_3 for Yb, and $LiNbO_3$ for Nb. The analyses were made using the Rb Lα and P Kα lines measured with the Thalium Acid Phthalate (TAP) crystal, the Ti Kα and Nb Lα lines measured with the Pentaerythritol (PET) crystal, the O Kα line measured with a W/Si multilayer crystal (2d = 60 Å), and the Yb Lα line measured with the LiF crystal. The measurements were integrated for 10 s for Rb, Ti, P, and O and 30 s for Yb and Nb, obtaining an accuracy of 1.3% for Rb, 1.4% for P, 2.5% for O, 0.9% for Yb, and 9.6% for Ti. We corrected the raw intensities for the effects of dead time, background, and matrix using the Pouchou and Pichoir (PAP) correction procedure.[9]

X-ray Diffraction. A colorless as grown single crystal of $Rb_3Yb_2(PO_4)_3$ was used for indexing and intensity data collection on an Enraf-Nonius CAD4 four-circle diffractometer. The structure was resolved by Patterson synthesis, using SHELXS97 utility,[10] and refined by a full-matrix least-squares method with SHELXL97 computer utility.[10] Information regarding crystal data, data collection, and refinement are given in Table 2, atomic coordinate information is given in Table 3, and anisotropic displacement parameters are given in Table 4.

Table 2. Crystal Data, Data Collection, and Refinement of $Rb_3Yb_2(PO_4)_3$

crystal data	
$Rb_3Yb_2(PO_4)_3$	Mo Kα radiation
formula weight = 887.40	λ = 0.710 69 Å
cubic	cell parameters from 25 reflections
$I2_13$	$\theta = 12-21°$
a =16.8700(10) Å	μ = 28.033 mm^{-1}
$\alpha = \beta = \gamma = 90°$	T = 293(2) K
V = 4801.1(5) $Å^3$	prismatic crystal
Z = 16	0.3 × 0.2 × 0.2 mm
D_x = 4.911 Mg m^{-3}	colorless
D_m = (not measured)	
data collection	
Enraf-Nonius CAD-4 diffractometer	R_{int} = 0.0556
$w-2\theta$ scan	θ_{max} = 30.02°
absorption correction: φ scan	$h = -16 \rightarrow 16$
6338 measured reflections	$k = -16 \rightarrow 16$
2282 independent reflections	$l = 0 \rightarrow 23$
1737 reflections with $I > 2\sigma(I)$	3 standard reflections; frequency 120 min; intensity decay, none
refinement	
refinement on F^2	$\Delta\rho_{max}$ = 0.484 e $Å^{-3}$
$R[F^2 > 2\sigma(F^2)] = 0.0410$	$\Delta\rho_{min}$ = −0.360 e $Å^{-3}$
$wR(F^2) = 0.0793$	
S = 0.869	
2282 reflections	
125 parameters	twin crystals, twin law m perpendicular to a
	BASF = 0.76
	Flack absolute structure parameter = 0.00(8)
$w = 1/[\sigma^2(F_o^2) + (0.0000P)^2 + 0.0000P]$ where $P = (F_o^2 + 2F_c^2)/3$	scattering factors from *International Tables for Crystallography*, Vol. C
$(\Delta/\sigma)_{max}$ = 0.004	

Table 3. Atomic Coordinates and Equivalent Isotropic Displacement Parameters of $Rb_3Yb_2(PO_4)_3$

atom	Wyckoff position	x	y	z	U(eq)
Yb(1)	8a	0.7507(1)	0.7507(1)	0.7507(1)	0.016(1)
Yb(2)	12b	1.0000	0.7500(1)	0.5355(1)	0.017(1)
Yb(3)	12b	0.5000	0.7500	0.9644(1)	0.016(1)
Rb(1)	12b	0.7500(1)	0.7529(3)	0.5000	0.035(1)
Rb(2)	12b	0.7461(3)	1.0000	0.7500	0.027(1)
Rb(3)	8a	0.8783(2)	0.8783(2)	0.8783(2)	0.037(1)
Rb(4)	8a	0.6218(2)	0.6218(2)	0.6218(2)	0.027(1)
Rb(5)	8a	0.5007(4)	0.9993(4)	1.0007(4)	0.049(1)
P(1)	24c	0.8891(4)	0.6500(4)	0.8810(3)	0.029(2)
P(2)	24c	0.6181(4)	0.6107(4)	0.8480(3)	0.027(2)
O(1)	24c	0.8489(9)	0.7024(10)	0.8130(9)	0.032(3)
O(2)	24c	0.8219(9)	0.6027(9)	0.9146(8)	0.028(3)
O(3)	24c	0.9520(12)	0.5926(12)	0.8464(11)	0.026(4)
O(4)	24c	0.9294(12)	0.7081(9)	0.9340(10)	0.037(3)
O(5)	24c	0.6688(9)	0.6461(11)	0.7858(11)	0.024(3)
O(6)	24c	0.6633(11)	0.5611(12)	0.9051(12)	0.029(4)
O(7)	24c	0.5650(9)	0.5448(7)	0.8149(8)	0.037(3)
O(8)	24c	0.5601(9)	0.6720(10)	0.8861(10)	0.032(3)

We recorded X-ray powder diffraction data of $Rb_3Yb_2(PO_4)_3$ to study the linear thermal expansion tensor of $Rb_3Yb_2(PO_4)_3$ with a Siemens D5000 powder diffractometer with a graphite monochromatized Cu Kα radiation. We used a $\theta-\theta$ goniometer using Bragg−Brentano parafocusing geometry and a scintillation counter as the detector. The diffractometer was equipped with an Anton-Paar HTK10 platinum ribbon heating stage. The cell parameters of the crystals were calculated from the powder diffraction data, which were collected with a step scan procedure in the range of 2θ =

(9) Pouchou, J. L.; Pichoir, F. *Rech. Aerosp.* **1984**, *3*, 13.
(10) Sheldrick, G. M. *SHELXS97* and *SHELXL97*; University of Göttingen: Göttingen, Germany, 1997.

Table 4. Anisotropic Displacement Parameters (Å²) of Cubic $Rb_3Yb_2(PO_4)_3$ [a]

atom	U_{11}	U_{22}	U_{33}	U_{23}	U_{13}	U_{12}
Yb(1)	0.016(1)	0.016(1)	0.016(1)	0.002(1)	0.002(1)	0.002(1)
Yb(2)	0.015(1)	0.017(1)	0.019(1)	0	0	0.003(1)
Yb(3)	0.020(1)	0.018(1)	0.010(1)	0	0	0.002(1)
Rb(1)	0.042(3)	0.030(2)	0.031(2)	0	−0.001(2)	0
Rb(2)	0.021(2)	0.025(2)	0.034(2)	0.004(2)	0	0
Rb(3)	0.037(1)	0.037(1)	0.037(1)	−0.003(2)	−0.003(2)	−0.003(2)
Rb(4)	0.027(1)	0.027(1)	0.027(1)	0.002(1)	0.002(1)	0.002(1)
Rb(5)	0.049(1)	0.049(1)	0.049(1)	0.005(1)	−0.005(1)	0.005(1)
P(1)	0.022(3)	0.039(3)	0.026(2)	0.004(2)	−0.004(2)	0.002(2)
P(2)	0.028(3)	0.022(3)	0.030(2)	0	−0.003(2)	0.002(3)
O(1)	0.033(6)	0.035(6)	0.028(6)	0.008(5)	0.012(5)	0.0015(5)
O(2)	0.021(5)	0.023(6)	0.040(8)	0.020(6)	−0.011(5)	−0.006(4)
O(3)	0.018(5)	0.028(7)	0.032(7)	0.006(5)	0.005(5)	0.009(5)
O(4)	0.034(6)	0.045(7)	0.034(5)	−0.013(5)	−0.011(5)	−0.003(5)
O(5)	0.018(6)	0.030(6)	0.025(6)	0.003(4)	−0.001(5)	−0.001(5)
O(6)	0.023(6)	0.039(10)	0.025(7)	0.019(6)	0.005(5)	0.008(6)
O(7)	0.041(7)	0.029(7)	0.042(7)	−0.010(5)	−0.012(5)	0.011(6)
O(8)	0.036(8)	0.025(6)	0.034(7)	−0.002(5)	0.001(5)	0.008(6)

[a] The anisotropic displacement factor exponent takes the form $-2\pi^2[h^2a^{*2}U_{11} + \ldots + 2hka^*b^* U_{12}]$.

10−70°. The step size was 0.03°, and the step time was 5 s. The structure of $Rb_3Yb_2(PO_4)_3$, determined by single-crystal X-ray diffraction, was used as the starting model for the calculation. These parameters were refined using the Rietveld method by the FULLPROF application.[11] The refinement was made by selecting a pseudo-Voigt function to describe individual line profiles. The final Rietveld refinement included an overall scale factor, background parameters, full width at half-maximum parameters, asymmetry parameters determining the shape of the Bragg peaks, a zero point for the Bragg angles, and the cell parameters.

Another series of X-ray powder diffraction measurements was taken to study the phase transitions of this material with temperature. The patterns were carried out using the previously mentioned equipment, but in this case we used a Braun position sensitive detector. The powder diffraction data were collected in the range of $2\theta = 10-70°$. The measuring time per degree was 10 s. We increased the temperature at a rate of 0.17 K/s and registered patterns every 50 K between 1273 and 1573 in heating and cooling cycles.

Differential Thermal Analysis (DTA) Measurements. Studies of possible phase transitions with temperature were analyzed by DTA, using a TA Instruments simultaneous differential techniques instrument SDT 2960. The experiments were carried out at 10 K/min in the range of 298−1673 K using Ar as the purge gas at a flow rate of 90 cm^3/min. The sample, weighing around 30 mg, was placed in a Pt pan. Calcined Al_3O_3 was used as the reference material. The experiments were carried out in heating and cooling cycles to obtain information about the reversibility of the different processes. The storage rate of data was in all cases 0.5 s/data point.

Second Harmonic Generation (SHG) Measurements. We studied the SHG response of $Rb_3Yb_2(PO_4)_3$ using the powder method.[12] Single crystals of $Rb_3Yb_2(PO_4)_3$ were powdered and graded using standard sieves to obtain particle of uniform size between 5 and 20 μm. Powders were placed in a 2 mm thick quartz cell and packed uniformly. A beam of $\lambda = 1064$ nm, generated by a pulsed YAG:Nd laser, incided on the sample. We measured the power of the energy reflected, both the fundamental and the doubled frequency, with two different Si detectors. We selected the desired signal using interferometer filters. We then compared the power of the fundamental and doubled frequency signals, averaged over 100 laser shots. This provided information about the efficiency of the second harmonic process.

This information was only a relative value of the SHG efficiency of the sample, so we compared this result with that for KH_2PO_4 (KDP), whose SHG efficiency is well-known.[13]

Results and Discussion

Crystal Growth. Single $Rb_3Yb_2(PO_4)_3$ crystals of between a few micrometers and a few millimeters were grown. These crystals were obtained when we studied changes to the crystallization region of $RbTiOPO_4$ (RTP) in the $Rb_2O-P_2O_5-TiO_2$ system when doping with Nb^{5+} and Yb^{3+},[1] with an initial solution composition of 40.8-27.2-32.0 mol %, located inside the crystallization region of RTP.[14] The $Rb_3Yb_2(PO_4)_3$ crystals were obtained from different substitutions of TiO_2 with Yb_2O_3 and Nb_2O_5 in the above solution composition in agreement with Table 1, which lists the different levels of substitution of TiO_2 for which the $Rb_3Yb_2(PO_4)_3$ phase was obtained.

The $Rb_3Yb_2(PO_4)_3$ phase was obtained for solutions whose concentration of Yb_2O_3 was higher than 2.2 mol % substituting TiO_2 and containing Nb_2O_5. The higher the concentration of Nb_2O_5 in the solution, the less Yb_2O_3 we needed to add to obtain the $Rb_3Yb_2(PO_4)_3$. In solutions without Nb_2O_5, the temperature of homogenization of the solution was so high that it was impossible to homogenize the solutions with the furnaces we used in the solution compositions in which this phase could appear. The Nb_2O_5 in the solutions decreased the temperature of homogenization. In this way we were able to homogenize them and obtain the first phase that crystallized by decreasing the temperature.

When we studied initial solutions that were rich in Rb_2O and P_2O_5,[1] we obtained the langbeinite phase[2] with chemical composition $Rb_2Ti_{2-x}Yb_x(PO_4)_3$ instead of the $Rb_3Yb_2(PO_4)_3$ phase. It appears, therefore, that this phase was stabilized in solutions that contained a high concentration of TiO_2 and low concentrations of Rb_2O and P_2O_5. However, to stabilize the $Rb_3Yb_2(PO_4)_3$ phase, we needed more Yb_2O_3 in the solution than we did with the langbeinite phase.

As Table 1 shows, for low concentrations of Nb_2O_5 we obtained the $Rb_3Yb_2(PO_4)_3$ phase. However, when the Nb_2O_5 concentration took a value of 1.28 mol %, the langbeinite phase appeared instead of the $Rb_3Yb_2(PO_4)_3$ phase.

EPMA Measurements. The chemical composition of these crystals was analyzed by EPMA. The most important feature in the chemical composition was that although $Rb_3Yb_2(PO_4)_3$ crystals were grown in solutions containing TiO_2 and Nb_2O_5, Ti was included only as a trace element and Nb was not incorporated into the crystals at all. Presumably this was because the concentration of Nb in the solution was less than that of Ti. The detection limits of these ions, measured by the EPMA technique, were 0.031 and 0.064 wt % for Ti and Nb, respectively, while the concentrations measured in these samples were 0.146 and 0.008 wt %. The concentration of Nb measured by EPMA was clearly lower than its detection limit. The large error in the

(11) Rodriguez-Carvajal, J. *Physica B* **1993**, *192*, 55.
(12) Kurtz, S. K.; Perry, T. T. *J. Appl. Phys.* **1968**, *39*, 3798.
(13) Dmitriev, V. G.; Gurzadyan, G. G.; Kikogosyan, D. N. *Handbook of Nonlinear Optical Materials*; Springer-Verlag: Berlin Heidelberg, 1991.
(14) Carvajal, J. J.; Nikolov, V.; Solé, R.; Gavaldà, Jna.; Massons, J.; Rico, M.; Zaldo, C.; Aguiló, M.; Díaz, F. *Chem. Mater.* **2000**, *12*, 3171.

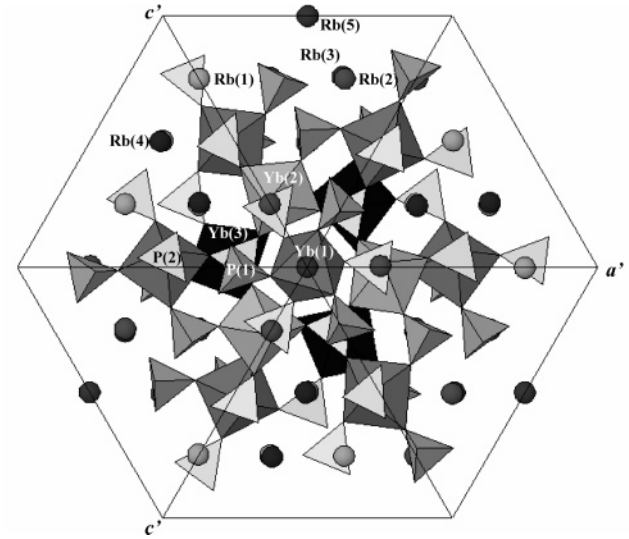

Figure 1. Projection of the structure of $Rb_3Yb_2(PO_4)_3$ along the [111] direction.

measurement of Ti and the low concentration of this ion led us to consider that Ti was only a trace element in the crystal.

We can see from these results that although the presence of Nb_2O_5 in the growth solution helps the crystallization of $Rb_3Yb_2(PO_4)_3$, supposedly by reducing the crystallization temperature of this phase, Nb is not included in the structure of the crystal. This situation was not observed in other phosphates of Rb and lanthanides such as $RbTiOPO_4$:(Nb,Yb),[1] $Rb_2Ti_{2-x-y}Yb_xNb_y(PO_4)_3$,[2] or $RbTiPO_5$:(Nb,Yb).[15]

Crystal Structure. We refined the structure of $Rb_3Yb_2(PO_4)_3$. This is a cubic structure with unit cell parameters $a = 16.8700(10)$ Å and $Z = 16$ and space group of symmetry $I2_13$. This structure is completely new for the compounds of the $A_3^1B_2^{III}(X^VO_4)_3$ family.

Figure 1 shows a projection parallel to [111] of the cell contents of $Rb_3Yb_2(PO_4)_3$. This structure is a cubic phase that can be described as a three-dimensional framework of alternating, vertex-sharing YbO_6 and PO_4 polyhedra. Rubidium cations occupy interstices in the Yb/P/O framework. There were three structurally different crystallographic positions for ytterbium, five for rubidium, two for phosphorus, and eight for oxygen. One of the Yb (Yb(1)) and three of the Rb atoms (Rb(3), Rb(4), and Rb(5)) were located at threefold axes. The other Yb and Rb atoms were located at twofold axes, and P and O atoms were located at general positions (see Table 3).

Table 5 lists the main interatomic distances obtained in this structure. All Yb atoms were six-coordinated with oxygen atoms to form an octahedron with different Yb−O bond distances. $Yb(2)O_6$ and $Yb(3)O_6$ octahedra had three Yb−O distances between 2.154 and 2.212 Å in $Yb(2)O_6$

Table 5. Selected Interatomic Distances (in Å) in $Rb_3Yb_2(PO_4)_3$

Yb(1)−O(1)	2.124(16)	P(1)−O(1)	1.600(17)	Rb(1)−O(8)[d]	2.795(17)	Yb(1)−P(1)	3.644(6)
Yb(1)−O(5)	2.318(18)	P(1)−O(2)	1.497(16)	Rb(1)−O(5)[b]	2.907(18)	Yb(1)−P(2)	3.629(7)
		P(1)−O(3)	1.55(2)	Rb(1)−O(6)[b]	3.19(2)		
Yb(2)−O(7)[a]	2.154(14)	P(1)−O(4)	1.491(13)	Rb(1)−O(5)[d]	3.390(16)	Yb(2)−P(1)	3.643(6)
Yb(2)−O(2)[b]	2.199(14)					Yb(2)−P(2)	3.596(7)
Yb(2)−O(6)[b]	2.212(19)	P(2)−O(5)	1.48(2)	Rb(2)−O(1)[b]	2.901(16)	Yb(2)−P(2)	3.625(6)
		P(2)−O(6)	1.486(19)	Rb(2)−O(2)[d]	3.066(17)		
Yb(3)−O(8)	2.122(17)	P(2)−O(7)	1.533(16)	Rb(2)−O(3)[b]	3.252(19)	Yb(3)−P(1)	3.592(6)
Yb(3)−O(4)[c]	2.204(10)	P(2)−O(8)	1.562(17)	Rb(2)−O(4)[d]	3.287(13)	Yb(3)−P(1)	3.626(6)
Yb(3)−O(3)[d]	2.26(2)					Yb(3)−P(2)	3.653(7)
				Rb(3)−O(3)[e]	2.95(2)		
				Rb(3)−O(4)	3.141(13)	Yb(1)−Rb(3)	3.729(8)
				Rb(3)−O(1)	3.204(17)	Yb(1)−Rb(4)	3.768(7)
						Yb(1)−Rb(2)	4.2060(18)
				Rb(4)−O(5)	2.907(18)	Yb(1)−Rb(1)[b]	4.2299(19
				Rb(4)−O(7)[f]	3.155(12)		
				Rb(4)−O(6)[f]	3.20(2)	Yb(2)−Rb(2)[d]	3.553(5)
						Yb(2)−Rb(4)[h]	3.992(2)
				Rb(5)−O(3)[d]	3.119(18)	Yb(2)−Rb(1)	4.2600(4)
				Rb(5)−O(6)[g]	3.360(19)	Yb(2)−Rb(5)[i]	4.269(5)
				Rb(5)−O(7)[g]	3.406(17)		
						Yb(3)−Rb(1)[b]	3.568(6)
						Yb(3)−Rb(3)[c]	3.992(3)
						Yb(3)−Rb(5)	4.251(5)
						Yb(3)−Rb(2)[b]	4.2605(4)
						P(1)−Rb(1)	4.069(7)
						P(1)−Rb(2)[b]	3.488(7)
						P(1)−Rb(2)[d]	3.396(7)
						P(1)−Rb(3)[e]	3.953(7)
						P(1)−Rb(5)[j]	3.724(7)
						P(2)−Rb(1)[d]	3.376(8)
						P(2)−Rb(1)[b]	3.472(7)
						P(2)−Rb(4)[k]	3.956(7)
						P(2)−Rb(5)[g]	3.754(8)
						Rb(3)−Rb(2)[d]	3.725(4)
						Rb(3)−Rb(5)[c]	3.536(12)
						Rb(4)−Rb(5)[l]	3.578(12)

[a] $=y + 1/2, 3/2 - z, 1 - x$. [b] $= z, x, y$. [c] $= 3/2 - x, y, 2 - z$. [d] $= y, z, x$. [e] $= 2 - x, 3/2 - y, z$. [f] $= 1 - y, 3/2 - z, x$. [g] $= 1 - x, 3/2 - y, z$. [h] $= 3/2 - x, y, 1 - z$. [i] $= x + 1/2, y - 1/2, z - 1/2$. [j] $= x + 1/2, 3/2 - y, 2 - z$. [k] $= x, 1 - y, 3/2$ -z. [l] $= 3/2 - y, z, 2 - x$.

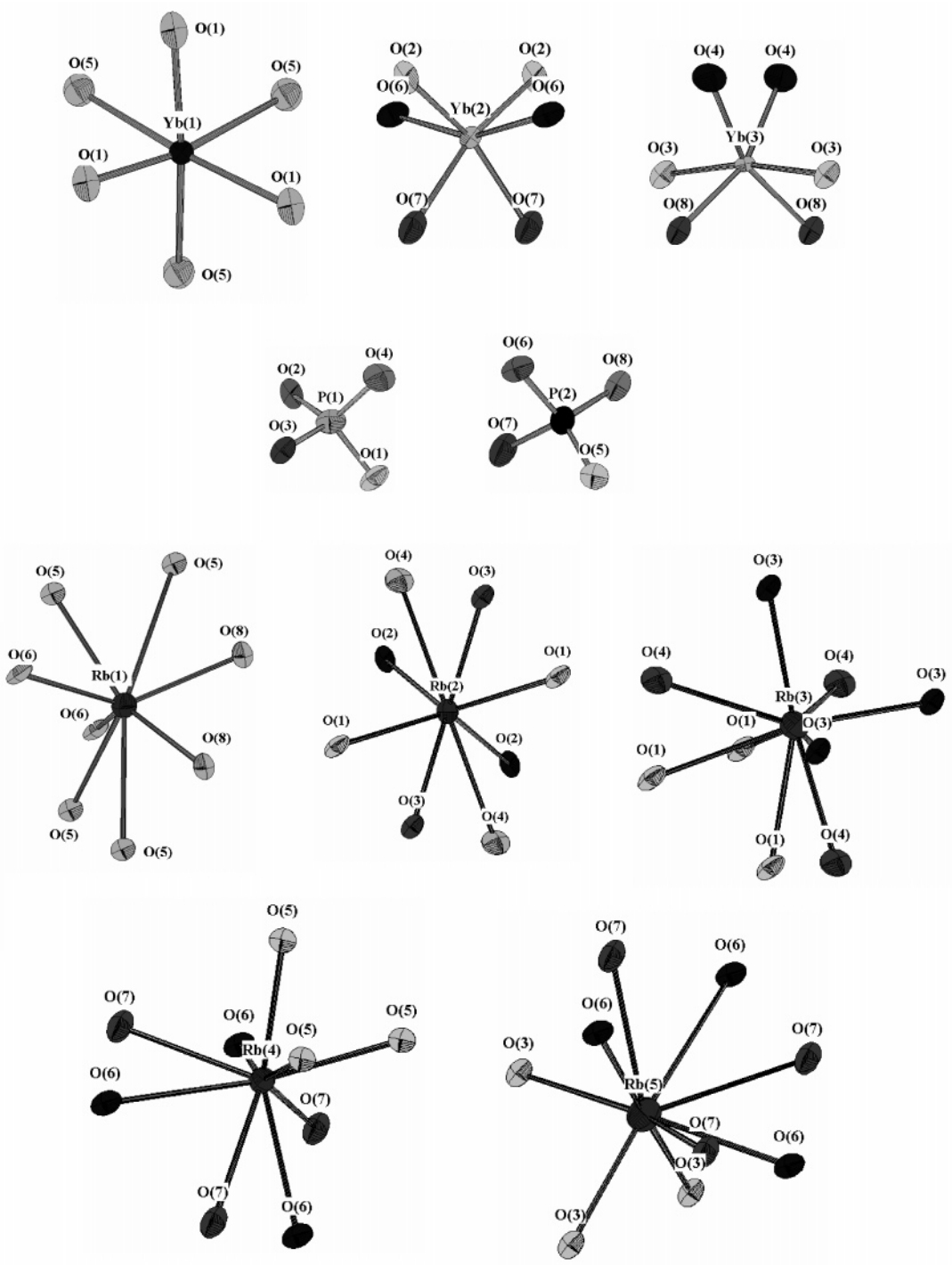

Figure 2. Details of the different coordination polyhedra in $Rb_3Yb_2(PO_4)_3$.

octahedron and 2.122 and 2.260 Å in $Yb(3)O_6$, while $Yb(1)O_6$, due to its special position, had only two Yb−O distances, between 2.124 and 2.318 Å. Corresponding to these bond distances $Yb(1)O_6$ had the greatest mean Yb−O bond distance (2.221 Å), while the mean Yb−O bond distances in $Yb(2)O_6$ and $Yb(3)O_6$ were lower and closer between them (2.188 and 2.195 Å, respectively), with the $Yb(3)O_6$ octahedron a little more expanded than the $Yb(2)O_6$ one. The distortions of the octahedra, defined as $\Delta^o = (1/6)\sum_{n=1,6}[(d_n^o - \langle d^o\rangle)/\langle d^o\rangle]^2$, where d_n^o are the Yb−O distances in the octahedron and $\langle d^o\rangle$ is the mean Yb−O distance calculated in each octahedron, were 19.07×10^{-4}, 1.29×10^{-4}, and 6.66×10^{-4} for $Yb(1)O_6$, $Yb(2)O_6$, and $Yb(3)O_6$, respectively. This shows that the $Yb(1)O_6$ octahedron was the most distorted and $Yb(2)O_6$ was the least. All these octahedra can be seen in great detail in Figure 2.

The P atoms were four-coordinated with oxygen atoms to form a slightly distorted tetrahedron. The P−O bond distances ranged from 1.491 to 1.600 Å in $P(1)O_4$ and from 1.480 to 1.562 Å in $P(2)O_4$. The mean P−O distance was higher for $P(1)O_4$ than for $P(2)O_4$ (1.534 and 1.515 Å, respectively), and $P(1)O_4$ was more distorted than $P(2)O_4$. Distortion was defined as $\Delta^t = (1/4)[d_n^t - \langle d^t\rangle/\langle d^t\rangle]^2$, where

(15) FiCMA. Unpublished results.

Table 6. Comparison of the Structure of the Compounds of the $A_3^IB_2^{III}(X^VO_4)_3$

compound	symmetry spatial group	cell parameters	ref
$Li_3Sc_2(PO_4)_3$	*Pcan*	$a = 8.853$, $b = 12.273$, $c = 8.802$	16
	$P112_1/n$	$a = 8.8483(4)$, $b = 12.2737(5)$, $c = 8.7959(4)$, $\gamma = 90.015(6)$	17
$Li_{2.8}(Sc_{1.8}Ti_{0.2})(PO_4)_3$	*Pbcn*	$a = 12.3332(4)$, $b = 8.7829(3)$, $c = 8.8067(3)$	18
$Li_{2.8}(Sc_{1.8}Zr_{0.2})(PO_4)_3$	*Pbcn*	$a = 12.3708(4)$, $b = 8.8086(3)$, $c = 8.8356$	18
$Li_{2.96}(Sc_{1.96}Zr_{0.04})(PO_4)_3$	$P112_1/n$	$a = 8.8572(3)$, $b = 12.2998(4)$, $c = 8.8183(3)$, $\gamma = 90.052(5)$	18
$Li_3Cr_2(PO_4)_3$	$R\bar{3}c$	$a = 8.272(2)$, $c = 22.219(5)$	8
	$P2_1/c$	$a = 8.453(1)$, $b = 8.547(1)$, $c = 14.520(2)$, $\beta = 125.15(1)$	8
	$P\bar{c}an$	$a = 8.829(1)$, $b = 12.397(1)$, $c = 8.821(2)$	19
$Li_3Fe_2(PO_4)_3$	$R\bar{3}c$	$a = 8.310(2)$, $c = 22.506(5)$	8
	$P12_1/c1$	$a = 8.568(1)$, $b = 8.613(1)$, $c = 14.690(1)$, $\beta = 125.16(1)$	8
	Pcan	$a = 8.592(2)$, $b = 12.129(2)$, $c = 8.637(2)$	20
	$P112_1/n$	$a = 8.562(2)$, $b = 12.005(3)$, $c = 8.612(2)$, $\gamma = 90.51(2)$	20
	$R\bar{3}$	$a = 8.3162(4)$, $c = 22.459(1)$	21
$Li_3In_2(PO_4)_3$	$R\bar{3}$	$a = 8.432(2)$, $c = 23.268(6)$	22
	$P12_1/n1$	$a = 8.592(2)$, $b = 8.908(2)$, $c = 12.290(3)$, $\beta = 90.0$	23
$Li_3Al_2(AsO_4)_3$	*R*	$a = 13.144(2)$, $c = 18.282(3)$	24
$Li_3Fe_2(AsO_4)_3$	*R*	$a = 13.665(2)$, $c = 18.439(6)$	24
	$P112_1/n$	$a = 8.608(1)$, $b = 12.215(1)$, $c = 8.929(1)$, $\gamma = 90.76(1)$	25
$K_3Al_2(PO_4)_3$	$Pna2_1$	$a = 8.685(2)$, $b = 16.947(2)$, $c = 8.458(3)$	33
$K_3Fe_2(PO_4)_3$	*C*2/*c*	$a = 16.303(2)$, $b = 9.463(1)$, $c = 16.691(2)$, $\beta = 118.39(1)$	8
$K_3Bi_2(PO_4)_3$	*C*2/*c*	$a = 13.828(7)$, $b = 13.482(5)$, $c = 6.808(3)$, $\beta = 114.94(4)$	34
$K_3Al_2(AsO_4)_3$	*R*	$a = 13.389(2)$, $c = 18.981(6)$	24
$K_3Fe_2(AsO_4)_3$	*R*	$a = 13.891(2)$, $c = 19.290(4)$	24
$Na_3Sc_2(PO_4)_3$	$R\bar{3}c$	$a = 8.950(2)$, $c = 22.230(4)$	27
	Bb	$a = 15.404(4)$, $b = 9.103(3)$, $c = 8.919(2)$, $\gamma = 123.53$	27
$Na_3Cr_2(PO_4)_3$	*C*2/*c*	$a = 14.959(1)$, $b = 8.655(1)$, $c = 8.748(1)$, $\beta = 124.53(1)$	28
	$R\bar{3}c$	$a = 8.643(2)$, $c = 21.619(3)$	26
$Na_3Fe_2(PO_4)_3$	*C*2/*c*	$a = 15.07(7)$, $b = 8.740(5)$, $c = 8.724(9)$, $\beta = 125.1(1)$	29
	$R\bar{3}c$	$a = 8.7270(2)$, $c = 21.8078(5)$	21
$Na_3In_2(PO_4)_3$	*C*2/*c*	$a = 12.450(1)$, $b = 12.786(1)$, $c = 6.5920(7)$, $\beta = 114.174(2)$	4
$Na_{3-x}K_xCr_2(PO_4)_3$	$R\bar{3}c$	$a = 8.567(1)$, $c = 22.654(6)$	8
$Na_{3-x}K_xFe_2(PO_4)_3$	$R\bar{3}c$	$a = 8.635(5)$, $c = 22.78(1)$	8
$Na_3Al_2(AsO_4)_3$	*C*2	$a = 14.576(6)$, $b = 13.409(6)$, $c = 9.728(5)$, $\beta = 96.95(4)$	7
$Na_3Ga_2(AsO_4)_3$	*R*	$a = 13.531(2)$, $c = 18.554(2)$	24
$Na_3In_2(AsO_4)_3$	*C*2/*c*	$a = 12.6037(2)$, $b = 13.1711(2)$, $c = 6.8342(1)$, $\beta = 113.743(1)$	4
$Na_3Al_{1.887}Y_{0.111}(AsO_4)_3$	$R\bar{3}c$	$a = 13.354(1)$, $c = 18.335(3)$	30
$Na_3Cr_2(AsO_4)_3$	$Ia\bar{3}d$	$a = 12.144(2)$	24
	R	$a = 13.553(2)$, $c = 18.557(4)$	24
$Na_3Sc_2(AsO_4)_3$	$R\bar{3}c$	$a = 9.2760(3)$, $c = 22.4640(8)$	32
$Na_3Fe_2(AsO_4)_3$	$R\bar{3}c$	$a = 13.698(5)$, $c = 18.590(6)$	31
	R	$a = 13.719(3)$, $c = 18.594(4)$	32
	$Ia\bar{3}$	$a = 12.222(3)$	32
$Ag_3Cr_2(PO_4)_3$	$R\bar{3}c$	$a = 8.698(2)$, $c = 22.009(4)$	8
$Ag_3Fe_2(PO_4)_3$	$R\bar{3}c$	$a = 8.772(1)$, $c = 22.113(2)$	8
$Ag_3Al_2(AsO_4)_3$	*R*	$a = 13.232(2)$, $c = 19.137(4)$	24
$Ag_3Fe_2(AsO_4)_3$	*R*	$a = 13.696(2)$, $c = 18.997(4)$	24
$Rb_3Al_2(PO_4)_3$	$Cmc2_1$	$a = 17.164(2)$, $b = 8.6270(6)$, $c = 8.8140(14)$	33
$Rb_3Sc_2(AsO_4)_3$	$Pa\bar{3}$	$a = 16.8749(7)$	35
$Rb_3Yb_2(PO_4)_3$	$I2_13$	$a = 16.870(1)$	

d_n^t are the P−O distances in the tetrahedron and $\langle d^t \rangle$ is the mean P−O distance calculated in each tetrahedron. The distortions were 8.31×10^{-4} and 5.01×10^{-4}, for $P(1)O_4$ and $P(2)O_4$, respectively. These tetrahedra are shown in more detail in Figure 2.

In terms of Yb−P−Yb topological connectivity, the YbO_6 octahedra shared all six corners with PO_4 tetrahedra at distances ranging from 3.5919 to 3.6535 Å. $Yb(1)O_6$ shared three corners with $P(1)O_4$ and three corners with $P(2)O_4$. $Yb(2)O_6$ shared two corners with $P(1)O_4$ and the other four corners with $P(2)O_4$. Finally, $Yb(3)O_6$ shared four corners with $P(1)O_4$ and the other two corners with $P(2)O_4$. For $Yb(2)O_6$ and $Yb(3)O_6$ we may say that the two corners shared with $P(1)O_4$ and $P(2)O_4$, respectively, were in a cis configuration, which means that these two corners were connected along one edge. The Yb−P distances depended on the YbO_6 octahedron and the PO_4 tetrahedron that are linked. For $Yb(1)O_6$, only two distances Yb−P were observed: 3.629 Å for P(1) and 3.644 Å for P(2). For $Yb(2)O_6$, the situation was different. We found only one distance for Yb(2)−P(1) (3.643 Å) but two distances for Yb(2)−P(2) (3.596 and 3.625 Å). Finally, for $Yb(3)O_6$, two distances were found for Yb(3)−P(1) (3.592 and 3.626 Å) and only one distance for Yb(3)−P(2) (3.653 Å). We can see that for both $Yb(2)O_6$ and $Yb(3)O_6$, which only shared two corners with $P(1)O_4$ and $P(2)O_4$, respectively, the distances Yb(2)−P(1) and Yb(3)−P(2) were the largest.

The PO_4 tetrahedra shared their four corners with YbO_6 octahedra and had an average Yb−O−P bond angle of 154.14°, which resulted from the vertex-sharing alternation of the YbO_6 and PO_4 polyhedra. The $P(1)O_4$ tetrahedron shared one corner with a $Yb(1)O_6$ octahedron, one corner with a $Yb(2)O_6$ octahedron, and two corners with $Yb(3)O_6$ octahedra, while the $P(2)O_4$ tetrahedron shared one corner with a $Yb(1)O_6$ octahedron, two corners with $Yb(2)O_6$ octahedra, and the last corner with a $Yb(3)O_6$ octahedron.

The most complex situation was that of Rb. The five structural sites of this atom in the structure occupy different coordination polyhedra with respect to nearby O atoms. All these polyhedra are described in Figure 2. Rb(1) had eight

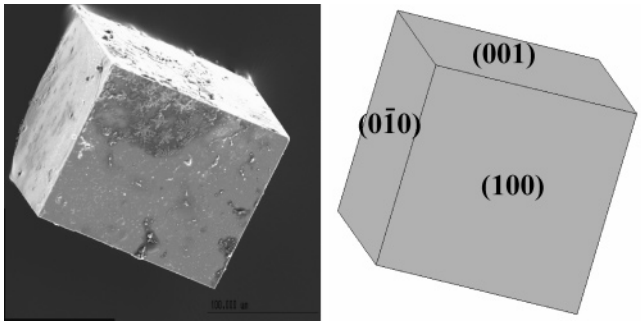

Figure 3. SEM photograph of a $Rb_3Yb_2(PO_4)_3$ crystal and morphological scheme.

atoms of oxygen at distances between 2.795 and 3.390 Å. Rb(2) had eight oxygen atoms at distances between 2.901 and 3.287 Å. Rb(3), Rb(4), and Rb(5) adopted a ninefold coordination with average Rb−O contact distances of 2.95 and 3.204 Å for Rb(3), 2.907 and 3.20 Å for Rb(4), and 3.119 and 3.406 Å for Rb(5).

Table 6 compares this structure with the other structures obtained in the family of $A_3^IB_2^{III}(X^VO_4)_3$ compounds, when only X = P and As were considered. Most of the compounds containing A = Na and X = P are known to be solid electrolytes that are structurally related to nasicon.[36] In the case of phosphates with A = Li, nasicon is the main structure, although polymorphism was observed in the case of B = Fe and Cr, with a structure related to that of $Fe_2(SO_4)_3$. When A = K, the phosphates belong to a modification of the garnet-type form. Some compounds, synthesized with A = Ag, have the NASICON structure. However, the corresponding arsenates (X = As) exhibit modifications: a rhombohedral form, widely generalized for any cation occupying the A positions, and also some polymorphism in the case of A = Na, with cubic and garnet-type forms. The only structure previously reported with A = Rb[35] crystallized in the cubic system. Table 6 clearly shows that no compound of the $A_3^IB_2^{III}(X^VO_4)_3$ family showed the structure of the $Rb_3Yb_2(PO_4)_3$ compound.

Table 7. *hkl* Reflections, d_{hkl}, 2θ-Bragg Position, and Their Observed Intensity in the X-ray Powder Diffraction Pattern of the $Rb_3Yb_2(PO_4)_3$ Crystal[a]

hkl	d_{hkl} (Å)	2θ-Bragg	I_{hkl}	*hkl*	d_{hkl} (Å)	2θ-Bragg	I_{hkl}
2 0 0	8.4442	10.468	1	8 4 0	1.8882	48.152	41
2 1 1	6.8946	12.829	4	8 3 3	1.8650	48.789	9
2 2 0	5.9709	17.824	>1	4 8 2	1.8427	49.420	12
1 3 0	5.3406	16.586	>1	6 5 5	1.8211	50.045	48
2 2 2	4.8752	18.181	151	6 6 4	1.8003	50.664	4
3 2 1	4.5136	19.652	38	5 7 4	1.7802	51.277	17
4 0 0	4.2221	21.024	165	6 7 3	1.7419	52.489	62
4 1 1	3.9806	22.315	24	8 4 4	1.7236	53.088	182
4 2 0	3.7763	23.539	12	8 5 3	1.7060	53.682	20
3 3 2	3.6006	24.706	33	8 6 0	1.6888	54.272	15
4 2 2	3.4473	25.823	8	7 7 2	1.6722	54.857	5
3 4 1	3.3121	26.896	73	6 8 2	1.6560	55.438	30
25 1	3.0834	28.933	90	4 9 3	1.6403	56.015	9
4 4 0	2.9855	29.904	999	6 6 6	1.6251	56.588	1
4 3 3	2.8963	30.847	6	3 10 1	1.6102	57.157	34
6 0 0	2.8147	31.764	6	8 5 5	1.5817	58.285	13
6 1 1	2.7396	32.659	66	4 10 0	1.5680	58.844	22
2 6 0	2.6703	33.532	9	6 9 1	1.5547	59.399	27
5 4 1	2.6059	34.385	21	10 4 2	1.5417	59.951	16
6 2 2	2.5460	35.221	1	7 8 3	1.5290	60.501	6
6 3 1	2.4900	36.039	9	10 5 1	1.5045	61.590	23
4 4 4	2.4376	36.842	64	8 8 0	1.4927	62.131	45
4 5 3	2.3884	37.630	1	10 4 4	1.4699	63.205	6
4 6 0	2.3420	38.404	8	7 7 6	1.4589	63.737	5
6 3 3	2.2982	39.165	29	8 6 6	1.4481	64.268	4
6 4 2	2.2568	39.914	18	8 7 5	1.4376	64.796	6
3 7 2	2.1448	42.094	13	6 10 2	1.4273	65.322	2
8 0 0	2.1110	42.800	96	8 8 4	1.4073	66.367	13
5 5 4	2.0788	43.498	45	8 9 1	1.3977	66.886	14
6 4 4	2.0480	44.186	24	2 12 0	1.3882	67.404	9
6 5 3	2.0185	44.866	55	5 11 2	1.3789	67.919	1
8 2 2	1.9903	45.538	15	12 2 2	1.3698	68.433	11
7 4 3	1.9632	46.202	33	9 8 3	1.3609	68.944	4
6 6 2	1.9372	46.859	6	10 7 3	1.3435	69.963	11
7 5 2	1.9122	47.509	7				

[a] The observed intensity has been normalized taking 999 as the most intense reflection.

Crystal Morphology. Several crystals of $Rb_3Yb_2(PO_4)_2$ were observed by SEM to describe their morphology. Only a cubic habit, made up of perfect squares and only comprising the {100} face, was observed. The habit of these crystals, grown by spontaneous nucleation on the surface of the solution to avoid partial morphologies, is shown in Figure 3 with a scheme drawn with the Shape utility.

However, in one of the faces of the crystal, dendritic precipitates were observed (see Figure 3), but we did not perform further analyses to determine the origin or composition of these depositions.

Thermal Expansion Coefficient. We studied the evolution of the *a* parameter of the $Rb_3Yb_2(PO_4)_3$ by X-ray powder diffraction in the 300−800 K temperature range using the Rietveld method by the FULLPROF program. As there was no powder diffraction file corresponding to this structure in the PDF−ICDD database,[37] Table 7 lists the (*hkl*), d_{hkl}, 2θ-Bragg position, and corresponding I_{hkl} observed, at room temperature.

(16) Kondratyuk, I. P.; Sirota, M. I.; Maksimov, B. A.; Muradyan, L. A.; Simonov, V. I. *Kristallografiya* **1986**, *31*, 488.
(17) Suzuki, T.; Yoshida, K.; Uematsu, K.; Kodama, T.; Toda, K.; Ye, Z. G.; Ohashi, M.; Sato, M. *Solid State Ionics* **1998**, *113*−*115*, 89.
(18) Sato, M.; Suzuki, T.; Yoshida, K.; Uematsu, K.; Toda, K.; Ye, Z. G. *J. Alloys Compd.* **1997**, *250*, 510.
(19) Genkina, E. A.; Maksimov, B. A.; Sigarev, S. E.; Verin, I. A. *Sov. Phys. Crystallogr.* **1991**, *36*, 352.
(20) Bykov, A. B.; Chirkin, A. P.; Demyanets, L. N.; Doronin, S. N.; Genkina, E. A.; Ivanov-Shits, A. K.; Kondratyuk, I. P.; Maksimov, B. A.; Mel'nikov, O. K.; Muradyan, L. N.; Simonov, V. I.; Timofeeva, V. A. *Solid State Ionics* **1990**, *38*, 31.
(21) Masquelier, C.; Wurm, C.; Rodriguez-Carvajal, J.; Gaubicher, J.; Nazar, L. *Chem. Mater.* **2000**, *12*, 525.
(22) Genkina, E. A.; Muradyan, L. A.; Maksimov, B. A.; Merinov, B. V.; Sigarev, S. E. *Sov. Phys. Crystallogr.* **1987**, *32*, 40.
(23) Tran Qui, D.; Hamdoune, S. *Acta Crystallogr., Sect. C* **1987**, *43*, 397.
(24) D'Yvoire, F.; Pintard-Screpel, M.; Bretey, E. *Solid State Ionics* **1986**, *18*−*19*, 502.
(25) Mesa, J. L.; Goni, A.; Brandl, A. L.; Moreno, N. O.; Barberis, G. E.; Rojo, T. J. *Mater. Chem.* **2000**, *10*, 2779.
(26) Genkina, E. A.; Kalinin, V. B.; Maksimov, B. A.; Golubev, A. M. *Kristallografiya* **1991**, *36*, 1126.
(27) Collin, G.; Comes, R.; Boilot, J. P.; Colomban, P. *J. Phys. Chem. Solids* **1986**, *47*, 843.
(28) Lucazeau, G.; Barj, M.; Soubeyroux, J. L.; Dianoux, A. J.; Delmas, C. *Solid State Ionics* **1986**, *18*−*19*, 959.
(29) Fanjat, N.; Soubeyroux, J. L. *J. Magn. Magn. Mater.* **1992**, *104*, 933.
(30) Belam, W.; Madani, A.; Driss, A.; Daoud, A. *J. Soc. Chim. Tunis.* **2000**, *4*, 735.
(31) Harrison, W.; Phillips, M. *Acta Crystallogr., Sect. C* **2001**, *57*, 2.
(32) d'Yvoire, F.; Bretey, E.; Collin, G. *Solid State Ionics* **1988**, *28*−*30*, 1259.
(33) Nandini Devi, R.; Vidyasagar, K. *Inorg. Chem.* **2000**, *39*, 2391.
(34) Falah, C.; Boughzala, H.; Jouini, T. *Z. Kristallografiya* **2001**, *216*, 493.
(35) Harrison, W. T. A.; Phillips, M. L. F.; Clegg, W.; Teat, S. J. *J. Solid State Chem.* **1998**, *139*, 299.
(36) Delmas, C.; Viala, J. C.; Olazcuaga, R.; Le Flem, G.; Hagenmuller, P.; Cherkaoui, F.; Brochu, R. *Solid State Ionics* **1981**, *3*−*4*, 209.

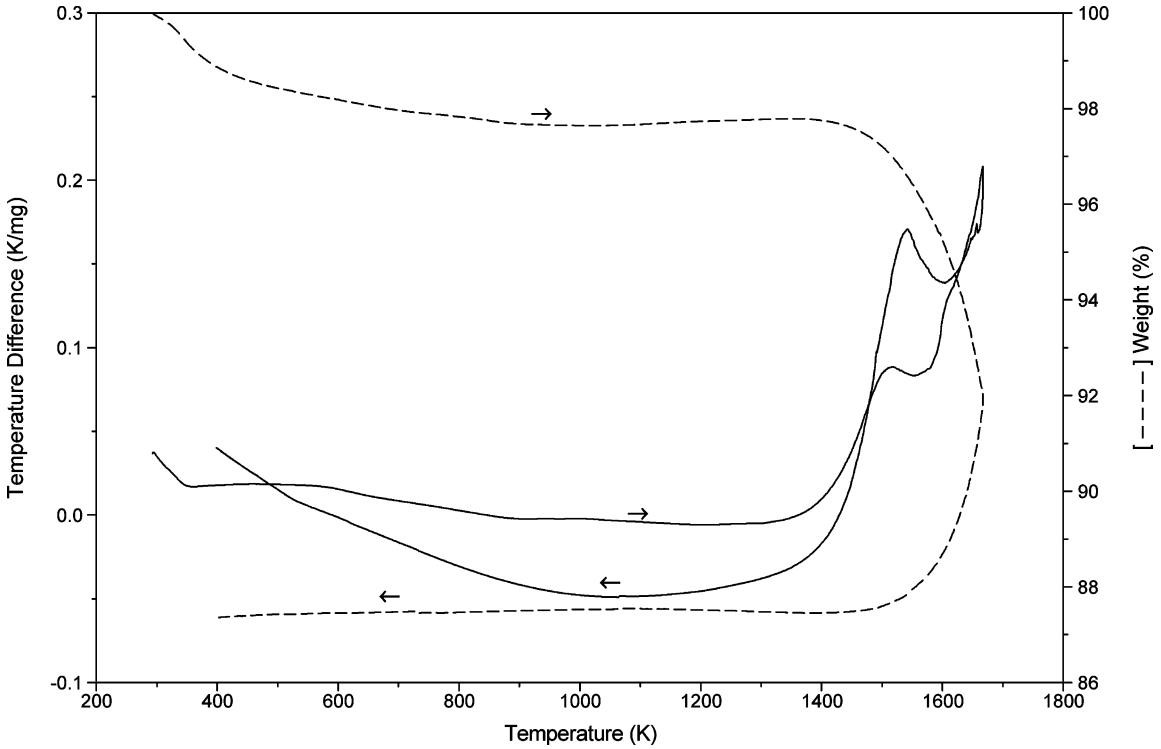

Figure 4. DTA (solid line) and TGA thermograms (dashed line) in the range between 298 and 1673 K.

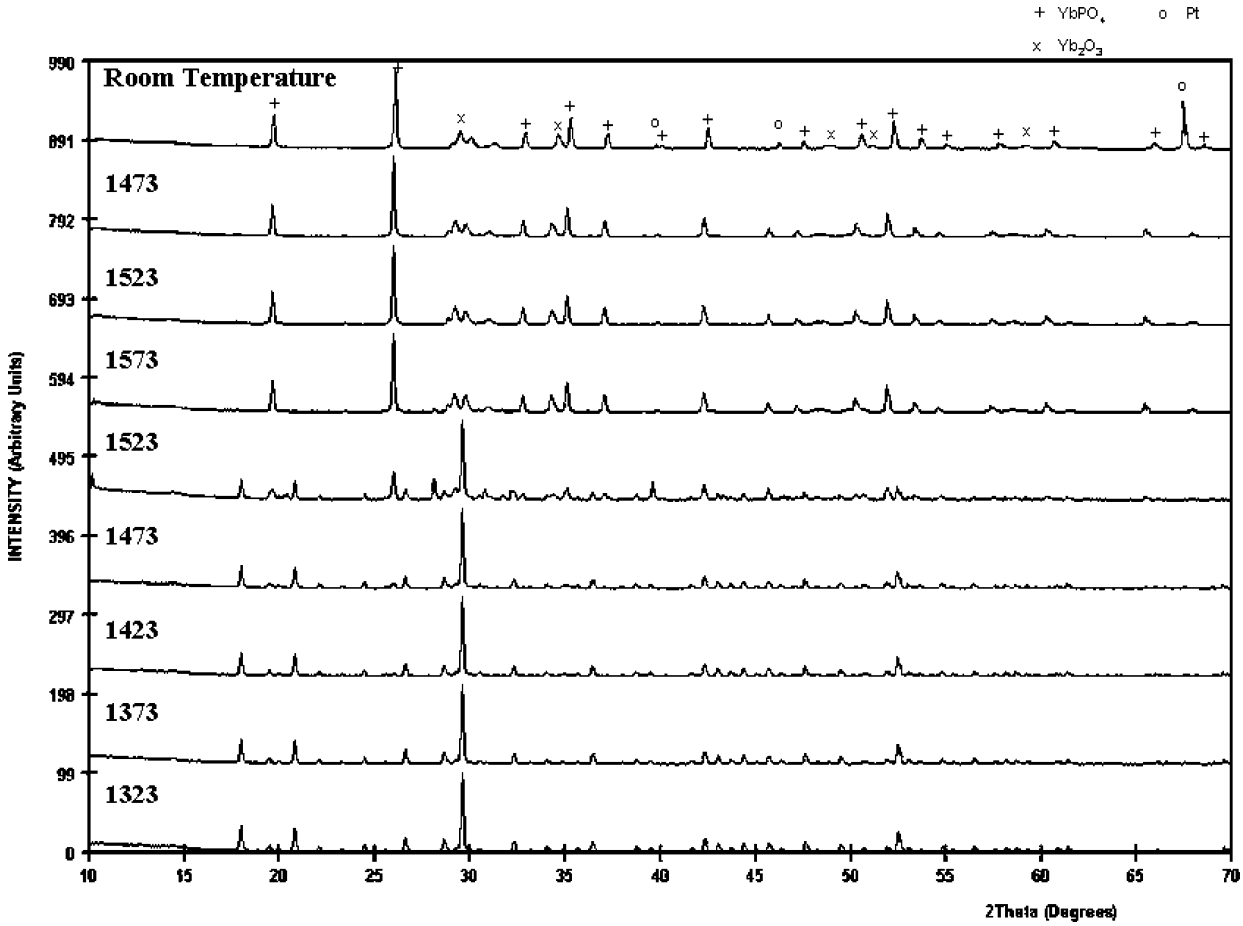

Figure 5. Selected X-ray powder patterns at different temperatures in the range between 1323 and 1573 K in heating and cooling cycles, describing the decomposition of $Rb_3Yb_2(PO_4)_3$ with temperature.

The linear thermal expansion coefficient, defined as $\alpha = (1/Y)(\Delta Y/\Delta T)$, with Y as the value of the a parameter at room temperature and ΔY as the change in this parameter when the temperature changes ΔT, was $\alpha = 8.94 \times 10^{-6}$ K^{-1}.

We can calculate this parameter from the slope of the linear fit of the linear relationship between ($\Delta Y/Y$) and the temperature of our measurements of the lattice parameter.

Stability of $Rb_3Yb_2(PO_4)_2$ with Temperature. We studied the stability of the $Rb_3Yb_2(PO_4)_3$ with temperature by DTA and X-ray powder diffraction. Figure 4 shows the DTA and thermal gravimetric analysis (TGA) thermograms of $Rb_3Yb_2(PO_4)_3$ in the 298−1673 K temperature range. We can see a large change in the slope of the signal associated with a loss of weight between 1450 and 1540 K. Then, a single and broad peak was observed at 1541 K. We studied these features in greater detail using X-ray powder diffraction, recording powder diffraction patterns at room temperature at the beginning and at the end of the experiment and at 50 K intervals between 1273 and 1573 K in heating and cooling cycles. Figure 5 shows the most interesting X-ray patterns obtained. At 1473 K the product of the decomposition of the $Rb_3Yb_2(PO_4)_3$ phase began to appear. This was identified as a mixture of $YbPO_4$ (45-0530, PDF−ICDD database)[37] and Yb_2O_3 (43-1037, PDF−ICDD database).[37] These phases were more evident at 1523 K. Finally, at 1573 K, the $Rb_3Yb_2(PO_4)_3$ disappeared completely and the products of the decomposition process were the only phases present in the diffractograms. The appearance of these new phases coincided with the change in the slope of the DTA signal. The peak observed in the DTA thermogram coincided with the complete change of the $Rb_3Yb_2(PO_4)_3$ by the $YbPO_4$ and Yb_2O_3 phases. The loss of weight in the sample may be related to the evaporation of the Rb_2O, though we cannot overlook the partial evaporation of P as P_2O_5, as observed in other related compounds.[2,38] In the cooling cycle, the $Rb_3Yb_2(PO_4)_3$ phase did not appear and only the $YbPO_4$ and Yb_2O_3 phases were detected. These data show the incongruent melting of the $Rb_3Yb_2(PO_4)_3$. We suggest the following reaction for the decomposition process, beginning at around 1450 K and ending at 1541 K:

$$Rb_3Yb_2(PO_4)_3 \rightarrow YbPO_4(s) + Yb_2O_3(s) + Rb_2O(g) + P_2O_5(g)$$

SHG. We analyzed the second harmonic response of the $Rb_3Yb_2(PO_4)_3$ crystal using the powder method.[12] We compared the SHG efficiency (η), defined statistically as the power of the signal whose frequency is twice that of the initial radiation divided by the power of the initial beam, with the efficiency of another nonlinear optical crystal widely used in optical applications, KDP. The result was $\eta/\eta_{KDP} = 1.37$, which indicates that the SHG of $Rb_3Yb_2(PO_4)_3$ is of the order of that of KDP. As KDP is actually the material that is most often used in industrial applications for SHG, further studies on the growth conditions and characterization of larger single crystals of $Rb_3Yb_2(PO_4)_3$ are justified. However, the applications of this crystal for SHG will be very limited because, as this crystal is cubic, it does not present birefringence. As a result phase matching is impossible for all multiple waves mixing processes such as three waves mixing. In addition, quasi phase matching processes are also forbidden because of the $Rb_3Yb_2(PO_4)_3$ symmetry, which does not belong to one of the 10 pyroelectric crystal classes, and, thus, the crystal cannot be ferroelectric.[39] We should point out that $Rb_3Yb_2(PO_4)_3$ is the only compound of the $A_3^IB_2^{III}(X^VO_4)_3$ family of materials for which optical activity has been reported.

Conclusions

We synthesized a new Yb-stoichiometric compound belonging to the $A_3^IB_2^{III}(X^VO_4)_3$ family using high-temperature solution methods. This opens up the possibility of new applications for this family of crystals in the field of laser emission. The fact that the $Rb_3Yb_2(PO_4)_3$ crystal shows nonlinear optical properties means that this new material can be used for self-frequency doubling and other applications related to its nonlinearity. To our knowledge, this is the first Yb-stoichiometric compound for which optical activity has been reported. Then, the usual applications of Yb-stoichiometric materials can be merged with that of the nonlinear optical materials increasing exponentially the possible applications for this new crystal. Further studies into the growth conditions of larger single crystals and accurate optical and spectroscopic studies are, therefore, justified.

Acknowledgment. The authors acknowledge CICyT for financial support of this work through Projects No. MAT2002-04603-C05-03 and MAT2005-06354-C03-02 and DURSI-Generalitat de Catalunya though 2001SGR-317 and 2005SGR-658. We also thank the Serveis Científico-tècnics of the Universitat de Barcelona for kindly supplying helpful measurements on EPMA.

CM0512934

(37) PDF−ICDD. Powder Diffraction File. International Center for Diffraction Data: Newton Square, PA, 2000.

(38) Carvajal, J. J.; Solé, R.; Gavaldà, Jna.; Massons, J.; Díaz, F.; Aguiló, M. *Chem. Mater.* **2003**, *15*, 2730.

(39) *International Tables for Crystallography*, 4th ed.; Kluwer Academic Publishers: Dordrecht, 1998; Vol. A.